Nuclear Materials and Energy 45 (2025) 101981

Contents lists available at ScienceDirect

Nuclear Materials and Energy

journal homepage: www.elsevier.com/locate/nme

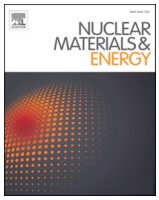

Influence of near-surface helium on the deuterium retention and uptake in tungsten☆

S. Markelj [a,*], T. Schwarz-Selinger [b], A. Šestan [a,c], J. Zavašnik [a,c], M. Kelemen [a]

[a] Jožef Stefan Institute, Jamova cesta 39, Ljubljana 1000, Slovenia
[b] Max-Planck-Institut für Plasmaphysik, Boltzmannstrasse 2, Garching D-85748, Germany
[c] Max-Planck-Institut für Nachhaltige Materialien, Max-Planck Strasse 1, Dusseldorf 40237, Germany

ARTICLE INFO

Keywords:
Helium
Deuterium retention
NRA
TDS
He bubbles
Displacement damage
Tungsten

ABSTRACT

The effect of near-surface helium (He) on deuterium (D) retention and uptake into the bulk of tungsten (W) was investigated. To quantify the He influence on D uptake, He was implanted close to the surface with 3 keV energy at different fluences and different temperatures. 20 MeV W irradiation was performed at room temperature after He implantation to create defects within the first 2.3 μm. Samples were then exposed to a low flux, low energy (300 eV/D) D ion beam at 450 K. The defects created by W ions trap penetrating D and make it hence possible to quantify D transport into depth below the He layer using ^{3}He nuclear reaction analysis. Elastic recoil detection analysis enabled us to measure the D and He concentration depth profiles near the surface. Results show that D gets preferentially retained where He is implanted with D concentrations up to 10 at.%. At the same time D uptake beyond the He zone is reduced by a factor of 15 compared to a He-free W sample.

1. Introduction

The presence of helium (He) in materials causes changes in macroscopic properties such as tensile strength, creep, fatigue behavior, swelling, and embrittlement [1,2]. In future fusion devices hydrogen isotopes deuterium (D) and tritium will be fused into helium to generate energy. Most of the 3.52 MeV α particles produced in the fusion reaction will be swept by the magnetic field and will gradually transfer its energy to the plasma species and will arrive at the wall with relatively low energy (20–100 eV) [5]. The 14.1 MeV neutron produced in the fusion reaction does not interact with plasma but will interact directly with the material causing radiation damage, and also initiating nuclear reactions leading to changes in the chemical composition of the materials. Many of these reactions produce gases, particularly He which is the second source of He in future fusion devices. The third source of He is its production through the decay of tritium due to tritium absorption and diffusion into the plasma-exposed material. Helium produced due to tritium decay or neutron-induced nuclear reactions (n,α) will have an effect throughout the bulk of the material. From the calculation by Shimada et al. [3] in the worst case scenario, assuming 1 at. % of tritium is retained in the wall, one can expect to get about 600 atomic parts per million (appm) of He to be created due to tritium decay. The contribution of He produced from the neutron-induced nuclear reactions depends very much on the choice of the wall material [4]. For tungsten (W), the primary material candidate for the first wall in future fusion devices, we can expect to get 30 appm after five full power years of neutron irradiation through neutron capture and alpha particle emission (n,α) in a fusion power plant [4]. One needs to stress that the emitted α particles have energies of the order of MeV, which means they will also cause displacement damage in the crystal lattice [2,4]. It is worth mentioning that transmutation of carbon produces He under neutron irradiation [4]. Therefore, carbon impurities in the tungsten material might even increase the predicted He concentration in the material in depth.

In our previous study [5] we investigated the effect of He on D retention and transport in the bulk of W. For this purpose samples were irradiated by 500 keV He ions at 300 K to different fluences in order to obtain He maximum concentrations of 1 at.%, 3.4 at.%, and 6.8 at.% in 0.84 μm depth. In order to discern the effect of irradiation damage caused by He implantation from the effect of the pure He presence on D retention, the W samples were irradiated at 290 K by 20 MeV tungsten ions in advance to create displacement damage in the crystal lattice to a

☆ This article is part of a special issue entitled: 'PFMC-20' published in Nuclear Materials and Energy.

* Corresponding author.
E-mail address: sabina.markelj@ijs.si (S. Markelj).

https://doi.org/10.1016/j.nme.2025.101981
Received 10 July 2025; Received in revised form 31 August 2025; Accepted 3 September 2025
Available online 5 September 2025

damage dose of 0.23 dpa. The samples were exposed to a D atom beam at 600 K with a flux of 3.5×10^{18}D/m^{2}s to populate all the created defects. We showed that D retention increased with implanted He fluence linearly following a D/He ratio of 0.29. We obtained peaking of D concentration at the position of maximum He concentration, reaching for the 6.8 at.% He sample three times higher D concentration (1.1 at. %) than obtained on high dpa W ion irradiated samples (0.37 at. %), for the same loading conditions. We have also demonstrated that He did not act as a diffusion barrier in either the as-implanted sample or the 1700 K annealed sample, where 2 nm bubbles were observed by transmission electron microscopy (TEM).

Here we focus on the effect that low energy He (eV to keV) can cause near the surface. According to literature low energy He will mainly affect the wall material by bubble growth and will alter deuterium (D) uptake and release at the surface [6,7]. It was experimentally shown that He influences the transport and retention of hydrogen isotopes (HI) close to the surface of the material [6]. Moreover, recent experiments studying the interaction of HIs and He in tungsten using He seeded D plasmas showed that the addition of He leads to reduced blistering [8,9]. Still, formation of nano-bubbles in the near surface layer was reported [8], which was accompanied by a reduced D retention [6]. The formation of these nano-bubbles by few eV to keV He ion irradiation is fluence and temperature dependent [7]. It was also shown that in sequential or simultaneous He^+ - D^+ ion implantations, D was trapped with He in the near surface region and D diffusion was limited only to the region where He was present [10]. While there were several attempts to explain the mechanisms for reduced blistering and reduced D retention, the actual cause for these observations is still a matter of discussion [11]. One proposed mechanism for the reduced D retention is *altered transport* where implanted He might create a diffusion barrier for D transport [8,11]. Second proposed mechanism is *altered recycling*, where nano-sized bubbles open-up additional pathways for D towards the surface thereby decreasing its transport into the bulk [9,11]. The conclusion of a recent detailed experimental and modelling effort concluded that probably both mechanisms of altered transport and altered recycling contribute to the He induced reduced hydrogen isotope retention effect in W [11]. Contrary to plasma experiments, increased D retention was observed experimentally in a recent study after thermal cycling of He-irradiated W samples where macroscopic bubbles were observed [12]. Increased D retention was experimentally found also in keV-range ion beam experiments [13,14] which seems to be in contradiction to what was observed in mixed He-D plasma exposures. However, the challenge of these studies [13,14] is that the applied He and D implantation energies cause displacement damage which is known to increase D retention in tungsten substantially. Therefore, one cannot distinguish unambiguously the influence of the presence of He from the displacement damage that the He creates. In all these studies where He is near the surface there is lack of quantitative depth profiling of He and D. The only quantitative depth profile measurement was performed by Lee at al. [10] and Shaw et al. [15] where in the first case elastic recoil detection analysis (ERDA) was used and in the second case laser ablation mass spectroscopy was performed to obtain D and He depth profiles in the tungsten samples exposed to He and D ions or He and D plasma, respectively. In both cased they have shown that D is trapped at the region where He is trapped, however no connecting study of the D uptake in quantitative manner was performed. Moreover, in a recent study Miyamoto *et al.* [16] showed that most of the D atoms were trapped and distributed homogeneously in the He bubbles.

There is also a number of theoretical studies addressing the interaction between He and HIs. Density functional theory (DFT) calculations show strong attraction between He and HIs [17,18], indicating preferential trapping of H around He clusters. Molecular dynamics (MD) simulations show that a large amount of H can be accommodated around He bubbles [19,20,21].

Moreover, it was shown by theory that He is very mobile in tungsten [22] but is easily and strongly trapped by vacancies or other defects [23] and tends to cluster with other He atoms [17,20]. Under certain conditions growth of He bubbles was observed, see e.g. [24] and references therein. This phenomenon itself is not yet fully understood, but is considered to be driven by He migration at high temperatures leading to bubble growth [24].

In the present study we apply a very similar methodology as we applied in our study in the bulk [5] to study the effect of helium at the surface to shed light on the question of how helium influences on the D retention and uptake. Our goal was to geometrically separate the three interaction regions, He implantation region, D implantation region and the region beyond both, where D can be trap. For this purpose, He was implanted close to the surface (10–20 nm) with 3 keV ions with different fluences at different temperatures. The He irradiation conditions were chosen such that we can expect, according to [7], He bubbles being visible by TEM. We have again used the 20 MeV W irradiation, creating defects within the first 2.3 μm that acts as a layer that traps D and "detects" if any D would migrate beyond the He surface layer. Namely, the defects created by W ions trap penetrating D and make it hence possible to quantify D transport beyond the He layer by detection of D using ^{3}He nuclear reaction analysis (NRA). Lastly, samples were exposed to a low flux, low energy (300 eV/D) D ion beam at 450 K, where implantation depth was shallower than the He implantation depth. ERDA was additionally applied to be able to detect both D and He at the same time at the very surface. Samples were also analysed by TEM to quantify the size and depth of possible He bubbles.

2. Experiment (Materials and Methods)

2.1. Sample preparation and exposure

In the experiment we used 12 × 15 mm^2 and 0.8 mm thick W samples cut from a hot-rolled polycrystalline W sheet with a purity of 99.997 wt% (Plansee). Grains are preferentially oriented parallel to the surface. Samples were mechanically and electro polished to a mirror-like finish [25] and then heated for 2 min in ultra-high vacuum at 2000 K for re-crystallization to reduce near-surface plastic deformations introduced by polishing and to ensure uniform, well-defined microstructure. This procedure enlarges the grain size to 10 – 50 μm [25,26].

Samples were irradiated by 3 keV He beam created by a commercial ion gun Gen-II from TECTRA (tectra.de) in the INSIBA setup at Jožef Stefan Institute (JSI), Ljubljana [27]. Two samples were implanted with a fluence of 3×10^{20} He/m^2 and 3×10^{21} He/m^2 at 300 K and one sample was exposed to a fluence of 3×10^{20} He/m^2 at 773 K. He fluence was calculated based on the visual beam spot on the sample that was 9 mm in diameter and on the ion current of 5–7 μA measured and monitored over irradiation time directly on the sample with 100 eV bias to compensate for the emission of secondary electrons. Although we did not measure the helium profile directly, we assume that the beam shape is a broad Gaussian. The possible slight different He fluence over the sample did not affect the behaviour of the D retention. Namely, we have measured the NRA signal after the D ion exposure with 2.4 MeV ^{3}He energy in the middle of the sample along the sample short axis, shown in Fig. 1c, and the signal was homogeneous except at the edges where no He was present, only W irradiation, showing increased D signal. According to SRIM 2008.04 code [28], He was implanted down to about 40 nm, as shown in Fig. 1 with a peak maximum at 11 nm. According to SRIM and assuming that all implanted He remains in the sample when it comes at rest, which is a theoretical upper bound, such 3 keV He irradiation leads to a He peak concentration of 15.6 at. % for the low fluence and 10 times larger for the high fluence, indicating the formation of bubbles.

After He irradiation, samples were irradiated by 20 MeV W ions to a fluence of 7.8×10^{17}W/m^2 at room temperature (290 K) in the TOF beamline [29] at the tandem laboratory of Max Planck Institute for Plasma Physics (IPP), Garching [29]. One sample was not irradiated by He and was irradiated only by W ions as reference, so-called "no He, self-dam. W". The W beam was scanned over the samples surface to achieve a laterally homogeneous irradiation. Using a displacement energy of 90

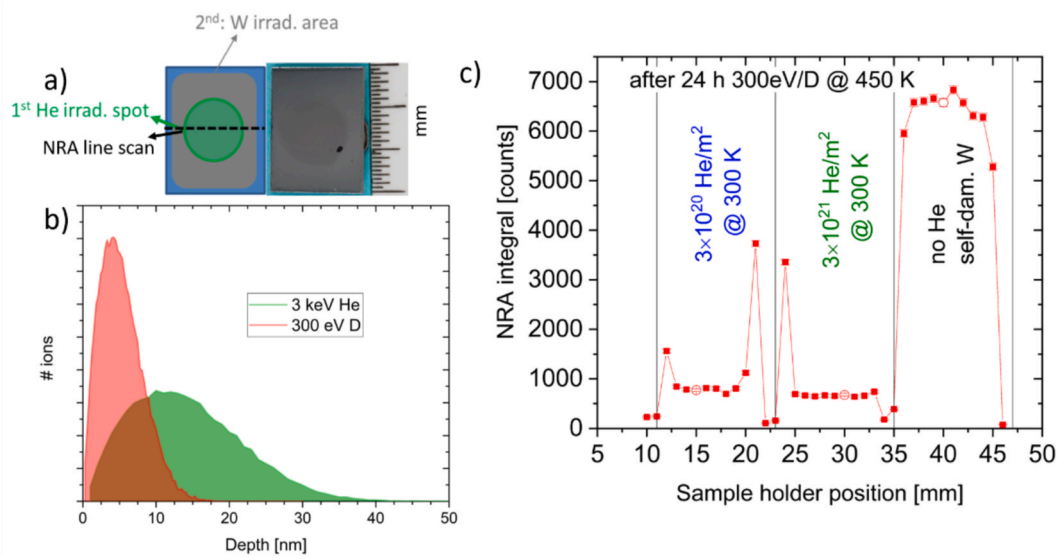

Fig. 1. a): schematic of W sample He and W irradiated area together with the photo of the He-irradiated sample. b) The implantation region of 3 keV He ions and 300 eV D ions as calculated by SRIM. c) NRA signal measured by ^{3}He beam at 2.4 MeV along the short samples axis on the two He samples irradiated at 300 K and on the no He, self-damaged W sample. Open circles mark the positions where D depth profiles were measured.

eV [30] and evaluating the "vacancy.txt" output of the "Ion Distribution and Quick Calculation of Damage" calculation option of the SRIM 2008.04 code [28] this creates a displacement-damaged zone extending down to 2.3 μm with a calculated primary peak damage dose of 0.23 dpa at a depth of 1.35 μm [29]. Preceding studies with the same tungsten material and the same damaging procedure showed that D retention saturates for this damage dose [31,32,33].

The He-irradiated and W-damaged W samples were exposed to deuterium (D) ions. The deuterium ion beam was also created with the same ion gun and setup as the initial helium implantation. The ion distribution at the operating conditions of the Gen-II source from TECTRA was quantified in detail in [34]. The flux is dominated by D_3^+ with small contributions of D^+ (3 %) and D_2^+ (0.7 %) [34]. The acceleration voltage applied to the ion gun was 1 kV and with 100 V bias on the sample, this then corresponds to 300, 900 and 450 eV/D ion energy, respectively. We can say with a high degree of certainty that the major D ion energy is 300 eV/D, given the negligible contributions of D_2^+ and D^+. The average D ion flux was $j = 2 \times 10^{18}$ m^{-2}s^{-1}. Samples were exposed for 24 h reaching a fluence of 1.7×10^{23} D/m^2. The sample irradiated to low He fluence at 300 K was again exposed for additional 48 h after the NRA analysis which resulted in a total D fluence of 5.2×10^{23}m^{-2}. The samples were in all cases exposed at 450 K. Fig. 1 shows the SRIM calculated implantation profile for 300 eV/D ions. According to SRIM [28] the distribution peaks at 5 nm and has maximum range of about 15 nm. Comparing with the He implantation profile in Fig. 1: one can see, the D ion energy is low enough that D ions are implanted closer to the surface as compared to He ions. The D beam spot was checked by erosion of an amorphous hydrogenated carbon (a-C:H) layer deposited on Si substrate and was larger than the He irradiation spot. The D exposure conditions were chosen such that no additional defects are created but only the existing defects are populated. The schematics of the He and W irradiated area is shown in Fig. 1 together with an image of the sample where the He irradiation spot is visible as a darker area. Both He and D beam were impacting perpendicular to the sample surface.

2.2. Analysis techniques

After the exposure to the D ion beam, NRA analysis was performed on all the samples utilizing a ^{3}He ion beam and the D(^{3}He,p)α nuclear reaction [35]. On the samples irradiated by He at 300 K and on the "no He", self-damaged W sample, first a line scan along the samples with 2.4 MeV ^{3}He beam with 1 mm sized beam in diameter and at 1 mm step was performed to check the homogeneity of the NRA signal, shown in Fig. 1**c**. This gives us the information about the retained D amount in the samples down to about 2.5 μm. One can observe that the NRA signal is very homogeneous along the He irradiation spot and there is an increase in the NRA signal at the edge on the He-irradiated samples. There we come to the region where only W damaging is present and as it can be observed on the no He sample, the NRA signal is higher and consequently also D retention is higher. The D depth profiles were measured in one position approximately in the middle of the samples, positions marked as open data points on individual samples in Fig. 1**c.** These measurements were performed at the standard NRA analysis beam line at IPP. In order to obtain a D depth profile [36] the proton signal from the nuclear reaction was measured at eight ^{3}He energies (500, 960, 800, 1200, 1800, 2400, 3200 and 4500 keV). Protons were detected by a 1.5 mm thick SiLi detector (called NRA detector) positioned at 135° with respect to the incoming probing beam with a geometrical solid angle of 78.7 msr. An additional alpha detector was used to measure the alpha particles from the nuclear reaction at low ^{3}He energies, up to 1200 K. The size of the probing beam was 1 mm in diameter positioned in the beam line. The beam impacts perpendicular on the sample surface. NRA depth profiling was also performed at JSI on the sample irradiated at 773 K as well on the low He fluence, 300 K sample after the additional D ion exposure. In those cases, measurements were performed in the INSIBA chamber in the middle of the sample following the D ion exposure. There we applied 6 beam energies (730, 1040, 1540, 2550, 3380, 4290 keV) with the NRA detector placed at 160° scattering angle and a geometrical solid angle of 26.69 msr [5]. In both cases (IPP and JSI) we also employed a detector to detect backscattered particles, the so-called RBS (Rutherford Backscattering Spectroscopy) detector, located at 165° with respect to the incoming beam. The signal from the RBS detector served to measure the absolute dose of ^{3}He particles impacting on the sample. In order to obtain from the NRA measurements one D depth profile, the proton energy spectra are first checked for energy calibration by SIMNRA [37] for all eight (six) measured energies. Cross section data published by Wielunska et al. [35] was used. These eight (six) energy spectra are then all input into NRADC [38] that outputs the most probable D depth profile. The uncertainties of the obtained D concentrations in the depth profiles are due to statistical errors that stem from the limited amount of counts we measured at each measuring ^{3}He beam energy and by the uncertainty of the D depth profile fit by NRADC. The

accuracy of the beam current measurement (typically 3–5 %) together with the counting statistics of about 1 % (counts depending on D content and energy) assures that the reproducibility of our measurements stays within 5 %. For our accumulated charge conditions, the detection limit of the NRA is about 1×10^{-3} at. %.

After NRA analysis the samples implanted with 3×10^{20} He/m^2 and 3×10^{21} He/m^2, both at 300 K, were analysed by ERDA using a O^{5+} beam at an energy of 15 MeV at the RKS chamber of the IPP tandem laboratory to detect both He and D near the surface. The schematic of the ERDA set up and the calibration procedure can be found in [39]. In short, the recoiled particles were collected at 30° recoil angle. A 5 μm Ni foil was placed in front of the detector. The aperture in front of the detector was curved with a calculated slit area of 1.539 mm^2 placed at a distance to the sample of 24.8 mm, corresponding to a geometrical solid angle of 2.5 msr.

The surface cross-sectional analyses were performed using a dual-beam Scanning Electron Microscope – Focus Ion Beam system (SEM-FIB, Helios NanoLab 650i, FEI Inc.). For cross-sectional preparation, the sample surface was first protected by a Pt deposit and then cut using Ga-ions at 20 kV and 100 pA. The features were visualised with secondary electrons collected by Everhart–Thornley detector at 15 kV and 0.80 nA. The same instrument was employed to prepare lamellae for TEM; initial shaping and thinning were carried out with 30 keV Ga^+ ions, followed by final polishing at 5 keV.

The morphology of the defects induced by MeV W and keV He ion irradiation were analysed by transmission electron microscope (TEM, JEM-2100, JEOL Inc.) operated at 200 kV. TEM micrographs were acquired with a slow-scan CCD camera (Orius SC-1000, Gatan Inc.) and processed by Digital Micrograph V3.01.and ImageJ software packages [40].

3. Results

3.1. Surface and cross-section analysis by SEM/FIB

The samples were examined both from the surface and in cross-section by SEM. Representative secondary electron micrographs are presented in Fig. 2. In the He-irradiated specimens the grain boundaries are well-defined with pronounced grain grooving. At higher magnifications, the surface of the reference sample appears smooth, whereas the He-irradiated samples show nanoscale "pores" with diameter of ~ 5 nm (see insets in Fig. 2), which we attribute to helium bubble formation. Focused ion beam (FIB) cross-sectional imaging reveals distinct contrast variations within the first ~ 50 nm from the surface in irradiated specimens, indicating structural modifications of tungsten. Such contrast changes are absent in the reference "no He" sample.

3.2. D and He retention results

3.2.1. Nuclear reaction analysis (NRA)

The derived D concentration profiles after D fluence of 1.7×10^{23} D/m^2 are shown in Fig. 3 in logarithmic scale as function of depth for all samples. The displacement damaged region is marked as grey shaded

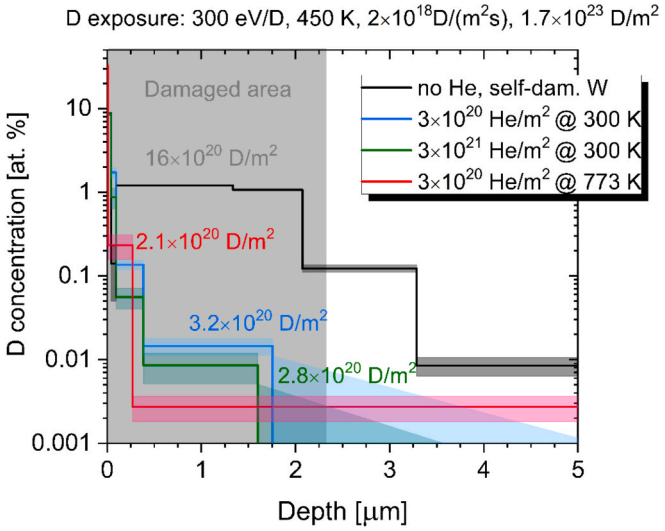

Fig. 3. D depth profiles obtained on the samples irradiated by 3 keV He beam at different He fluences and different temperatures. One sample was not exposed to 3 keV He beam but only to W ion beam and is used as a reference. All samples were irradiated by 20 MeV W ions at 290 K to create displacement damage and exposed to 300 eV/D ions at 450 K.

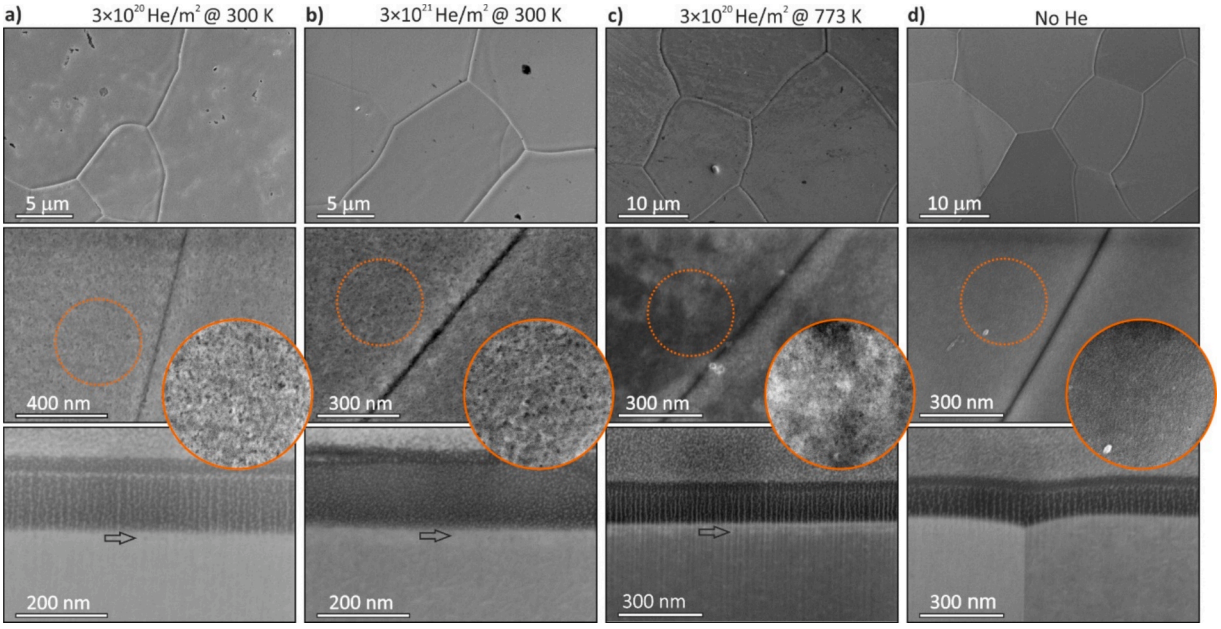

Fig. 2. (a-c) SEM micrographs of the surface and cross-sections of W samples exposed to He irradiation at different fluences and temperatures; (d) reference W sample without He exposure for comparison. Arrows indicate near-surface contrast variation associated with He bubble formation.

region. One can observe that in the sample only irradiated by W and exposed to D ions there is an increased D concentration down to about 2 μm with maximum D concentration of 1.2 at. % that drops down to 0.008 at. % beyond 3.3 μm. Such concentration beyond 3 μm is typical for D retention in non-irradiated polycrystalline W [34]. For the samples first irradiated by 3 keV He ions, then by W and last to D ions, the D depth profiles look very different. In these cases, D is found only near the surface with a D concentration averaged over the first 10 nm and then stepwise decrease down to 200 nm. The D concentration is 8 to 12 at. % at the surface and then decreases to about 1 at. % and reaches the level of non-irradiated D concentration at about 1 μm. Integrating the D depth profiles one gets the total retention within the information depth. Also, there is a large difference between non-helium and helium implanted samples. The total D amount in the only W irradiated W sample is 16 × 10^{20} D/m^2 while on the He irradiated samples is ≥ five times lower being 3.2 × 10^{20}D/m^2 for He fluence of 3 × 10^{20} He/m^2, 2.8 × 10^{21} D/m^2 for He fluence of 3 × 10^{21} He/m^2 at 300 K and 2.1 × 10^{20} D/m^2 for He fluence of 3 × 10^{20} He/m^2 at 773 K. One can also observe that the D retention is lower and D depth profile is narrower and closer to the surface for the 300 K high He fluence sample and the 773 K sample as compared to the low He fluence, 300 K sample. In Fig. 4 the D total amount is shown for the only W-irradiated sample and the sample additionally irradiated with 3 × 10^{20} He/m^2 for the two different D ion fluence. One can observe that even after two times higher D ion fluence the D total amount in the He sample is still four times lower compared to only W-irradiated sample. To get rid of the surface effects, we plot also the D retention beyond 40 nm. This amount is 3.5 times lower compared to the total D amount in the He-irradiated sample and tells us how much D amount penetrated beyond the He layer. This means that 15 times lower D transport beyond 40 nm is observed for the He-irradiated sample, compared to the only W-irradiated W sample.

3.2.2. *Elastic recoil detection analysis (ERDA)*

After the NRA analysis the He-irradiated samples at 300 K to a fluences of 3 × 10^{20} He/m^2 and 3 × 10^{21} He/m^2 were analysed by ERDA where both He and D can be measured at the surface at the same time. A measured ERDA spectrum using 15 Me V O^{5+} beam and a model curve using the SIMNRA program [37] are shown in Fig. 5 for the sample implanted by 3 × 10^{20} He/m^2. One can observe three peaks that can be from the recoil kinematics attributed to He, D and H. The protium comes from the water adsorbed on the surface due to the air exposure.

From the analysed spectra fitted by using SIMNRA, the obtained depth profiles from D and He are shown in Fig. 6**.** One can observe that exactly where He is detected also D is retained. The D/He ratio is 0.5 in both cases which is close to what we have obtained in the bulk [5]. The high fluence sample shows broader distribution of He and D compared to the low fluence sample. The total He and D amounts measured by ERDA in the low fluence sample are 2.7 × 10^{20} He/m^2 and 1.96 × 10^{20} D/m^2 and for the high fluence are 3.18 × 10^{20} He/m^2 and 2.0 × 10^{20} D/m^2. The He amount is in good agreement with the applied He fluence for the low sample but is an order of magnitude lower for the high fluence. The D amounts are about 30 % less as measured by NRA, however we need to point out that ERDA measurements were performed about a year after the NRA measurements and the low fluence sample was exposed to the additional D fluence, see Fig. 4.

3.3. *Transmission electron microscopy (TEM) analysis*

After D ion exposure, the samples were analysed by TEM to assess the presence and characteristics of He bubbles in the near-surface region. In all He-irradiated samples, a network of large, not-spherical bubbles was observed (Fig. 7**)**. The depth distribution of bubble sizes is summarised in Fig. 8**.**

The statistical parameters of bubble size distributions are summarised in Table 1. For samples irradiated at 300 K, the largest bubbles and highest bubble densities occur at a depth of ~ 15 nm. At a fluence of 3 × 10^{20} He/m^2, the mean bubble size is 2.2 nm, whereas at 3 × 10^{21} He/m^2 the mean size is reduced to 1.1 nm. The high fluence sample also shows nearly twice the bubble density within the first 30 nm compared to the low-fluence case.

At elevated temperature (773 K, fluence 3 × 10^{20} He/m^2), the peak density of the largest bubbles are found deeper at ~ 25 nm, with a mean size of 1.8 nm.

The depth distribution correlates well with the He and D profiles measured by ERDA; confirming that the regions with the largest and most abundant bubbles coincide with the highest He and D concentrations.

He bubble size distributions are also summarized in Fig. 7 (Feret diameters [41], area size, and bubble morphology). For the 300 K, 3 ×

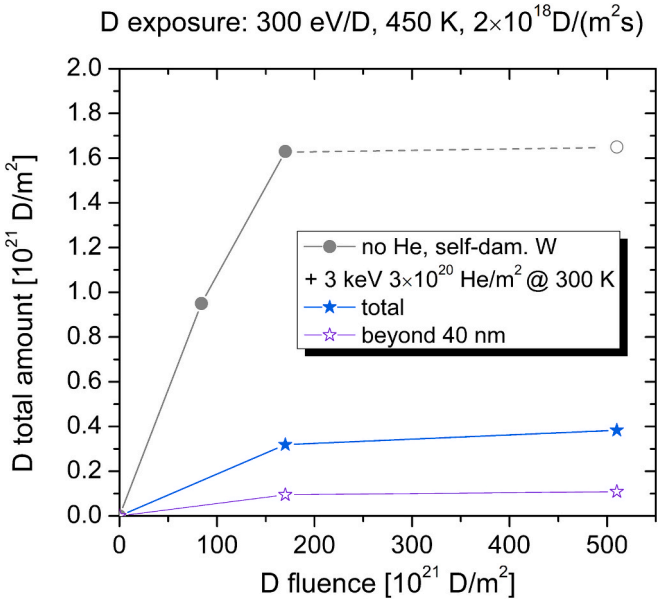

Fig. 4. D total amount as a function of D fluence for only W-irradiated sample and the He and W irradiated sample. The D amount beyond 40 nm is shown for the He-irradiated sample.

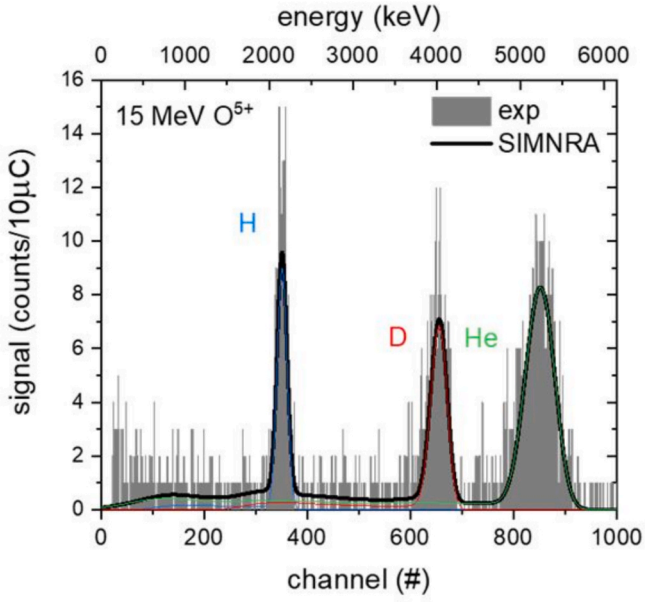

Fig. 5. The ERDA spectrum obtained on the sample irradiated by 3 × 10^{20} He/m^2 He fluence.

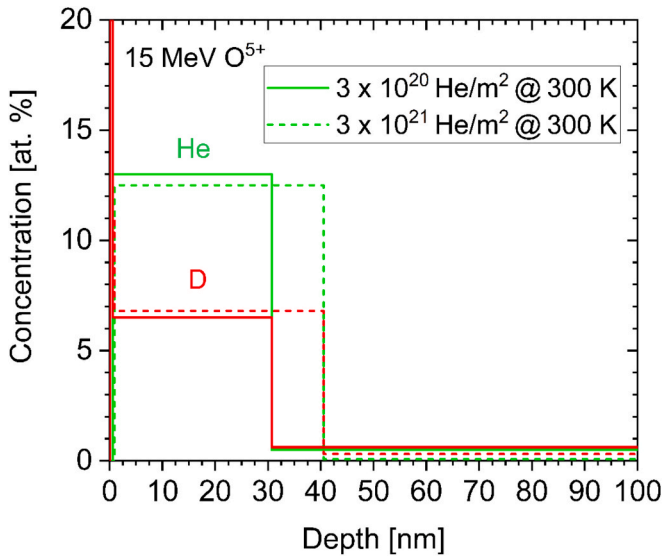

Fig. 6. Depth profiles of D and He as measured by ERDA. The W areal density was converted into a geometrical depth with an assumed density of 6.319 × 10^{22} W/cm^2.

10^{20} He/m^2 sample, bubble diameters range from 0.5 to 6.5 nm, with the mean size of 2.2 nm and a density of ~ 6000 bubbles/μm^2. At a higher fluence (3 × 10^{21} He/m^2, 300 K), the distribution narrows to 0.5 nm to 3.5 nm, with a few bubbles outliers up to 5 nm. The mean size of bubbles is 1.1 nm, with higher density of ~ 8375 bubbles/μm^2. In this case, the bubbles appear more spherical compared to the low fluence sample.

For the sample irradiated at 773 K (3 × 10^{20} He/m^2), the mean bubble size increases slightly to 1.7 nm, with a broader distribution of 0.5–6 nm. The bubble density is lower, ~5175 bubbles/μm^2, than in the 300 K case at the same fluence.

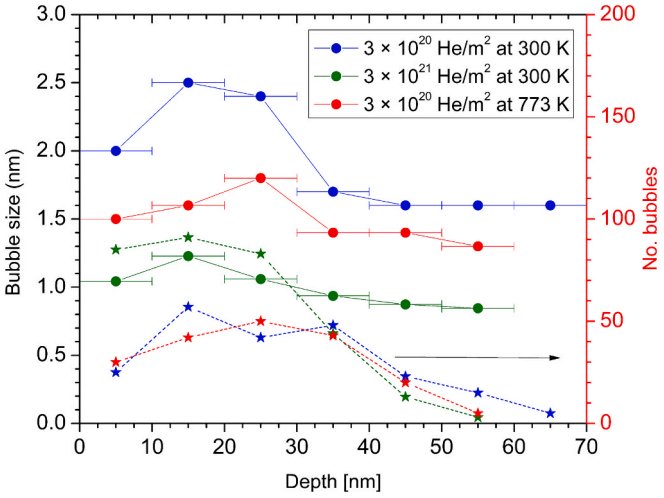

Fig. 8. Bubble size depth distribution (solid lines) is shown together with the number of bubbles in individual regions (dashed lines, right scale). The analysis was made in 10 nm depth regions.

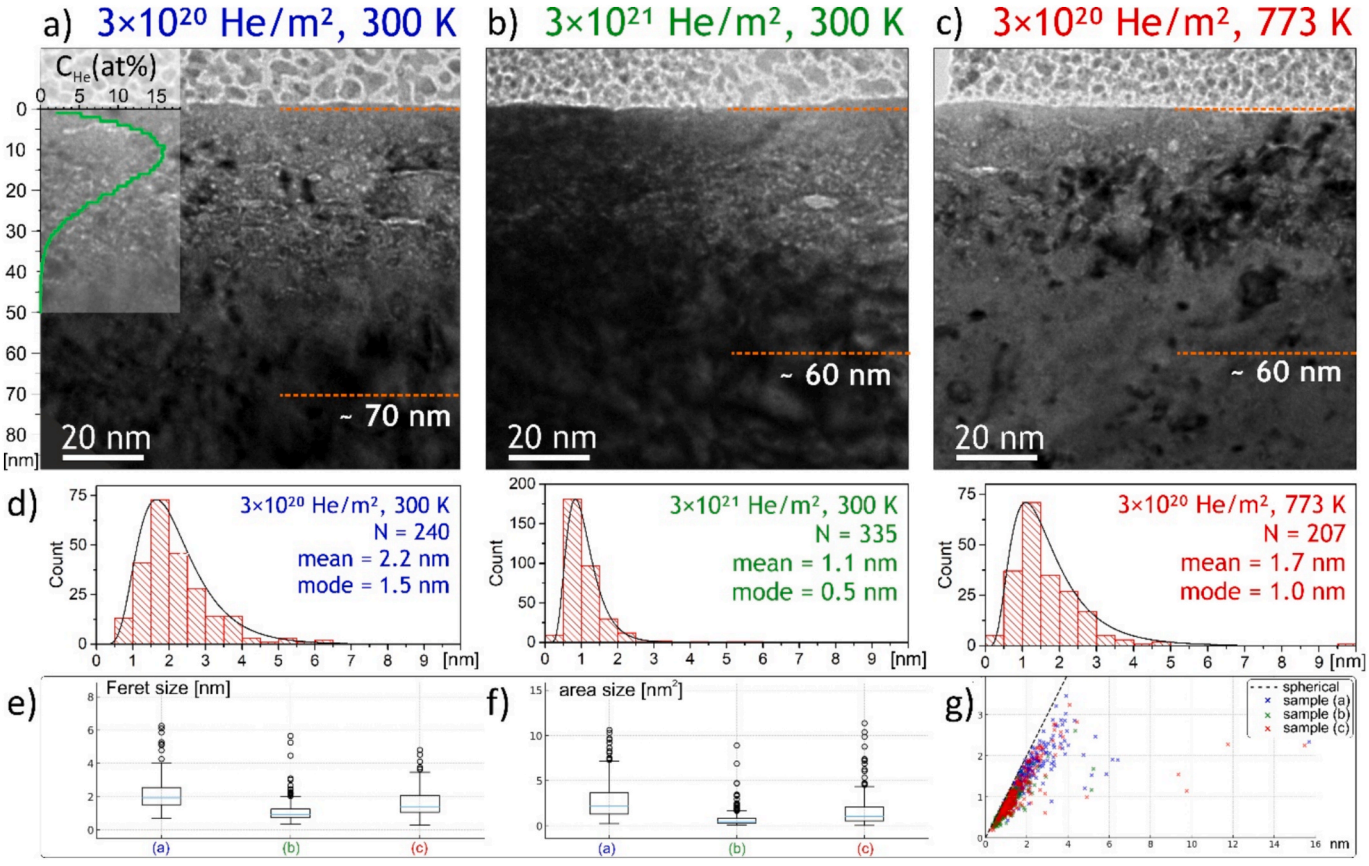

Fig. 7. (a-c) tem micrographs of He bubbles in W. The maximum depth of bubble occurence is indicated by the dashed orange line, with the SRIM-calculated He implantation depth profile overlaid. (d) Feret diameter size distribution of bubbles for the different He-irradiated samples. (e) Box plots of bubble Feret diameters and (f) bubble area. (g) Scatter plot of bubble minor versus major axes, showing elongation of the bubbles. (For interpretation of the references to colour in this figure legend, the reader is referred to the web version of this article.)

Table 1
Statistical parameters of bubble size distributions. "Mode" represents the most frequently observed bubble size, "Mean" is the arithmetic average, and "Std. Dev." denotes the standard deviation, i.e., the average scatter of values around the mean.

	sample	N (number of bubbles)	mode [nm]	mean [nm]	*Std. Dev.*
Sample 1	3×10^{20} He/m^2, 300 K	240	1.5	2.2	*0.97*
Sample 2	3×10^{21} He/m^2, 300 K	335	0.5	1.1	0.59
Sample 3	3×10^{20} He/m^2, 773 K	207	1.0	1.7	*0.97*

4. Discussion

We have studied how the presence of near surface He in tungsten influences D retention and uptake. In order to be able to evaluate the possible reduced D transport into depth the samples were additionally exposed to 20 MeV W ions. The traps created by W ions should act as a getter layer for D atoms that penetrate beyond the He irradiated layer. The samples were exposed to D ions with energy of 300 eV/D at 450 K. From SRIM calculations the D implantation depth is smaller as compared to He implantation depth. This is an important point since in case if D implantation would be deeper than the He depth, then the D retention and transport might be different. Experiments show that D hardly penetrates the few tens of nanometer thick He region whereas for the helium-free sample (only W-irradiated) D penetrates micrometers deep. Moreover, we have shown that D concentration locally increases exactly where He is implanted. TEM analysis revealed that for our irradiation conditions nm size bubbles are formed and the observed bubble size agrees very well with the observations by Miyamoto et al. [7]. We do observe some discrepancy between the 300 K and 773 K case where smaller bubble size is observed for the 773 K case. We interpret this as a balance between two processes: (i) enhanced He mobility at 773 K promotes He diffusion and bubble coalescence deeper in the material, reducing the number density near the surface, and (ii) partial He release at the elevated temperature lowers the retained He inventory near the surface. Thus, although bubbles coalescence (grow) at higher T, their reduced number density lead to an apparently smaller mean size in the analysed surface layer. In a separate study it was also shown that these bubbles do contain He atoms [16] which is agreement with our TEM and ERDA data showing He bubbles and He retention in the same depth region. This means that D is trapped at those He bubbles as was also observed in Miyamoto et al. [16]. We observed that the larger the He fluence the more effective is D trapping near the surface and less penetration beyond the He layer takes place. With increase of the He irradiation temperature the effect is even stronger, meaning that in the case of He irradiated at 300 K we still observe some D retention down to about 1.5 μm whereas in the sample irradiated at 773 K the D retention is observed only down to 300 nm.

We have for the first time showed that D is trapped with high concentration at the area where He and He bubbles are present and that the D uptake beyond this layer is reduced by more than a factor of four.

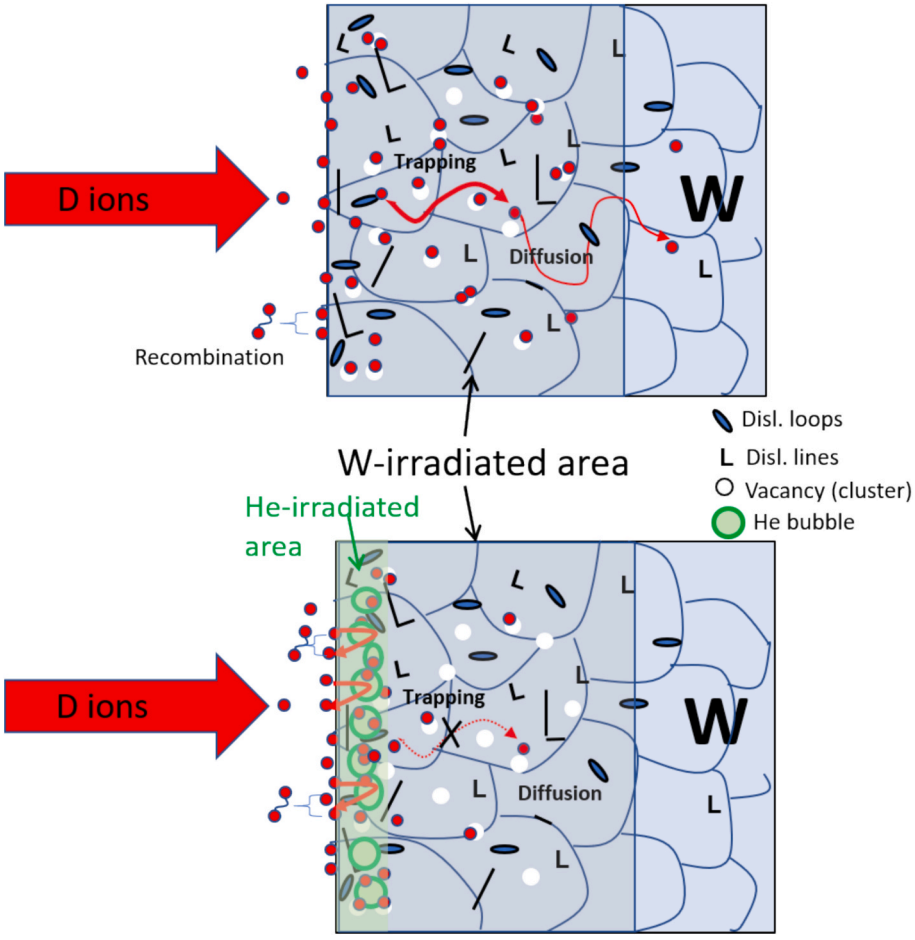

Fig. 9. Schematic of the processes taking place in only W-irradiated W and He- and W-irradiated W.

From the observed D retention, D uptake and microstructure studies we cannot confirm or disprove either of the two proposed mechanisms: altered transport or altered recycling, since we did not prove that we have an open porosity that could act as short-circuit path. But we can conclude that the D transport is changed in this highly corrugated He bubble layer where there is on one hand increased D trapping and at the same time the D transport beyond this layer is reduced. The increased D trapping agrees with our bulk studies [5] where we have clearly shown that He bubbles serve as trapping sites for D. However there we did observe D transport beyond the He bubble layer where also about 2 nm sized bubbles were observed. Here on contrary our NRA and ERDA results show that D accumulates at the He bubble layer (10–40 nm) with concentrations $>$ 10 at.% while penetration beyond this region is reduced by a factor of $\sim$ 15. This indicates that the bubble-rich layer is highly corrugated, with possible open pathways and high local trapping energy. We propose that this structure facilitates back-diffusion of D towards the surface where D can recombine and desorb more readily compared to transport into the bulk. Thus, although bubbles act as strong traps, they simultaneously act as scattering centres and diffusion "short-circuits" to the surface. This dual role explains the observed reduction of bulk uptake and is consistent with the "altered recycling" mechanism discussed in earlier plasma studies. We have created a schematic picture of the D transport with or without the He bubble layer at the surface in displacement damaged tungsten shown in Fig. 9. We have to stress that in both cases the D transport is slowed down and D concentration is increased due to trapping at the defects created by W ion irradiation and He bubbles but the He layer has the additional effect at the surface, as discussed above. Our conclusion is that the corrugated layer with He bubbles at the surface promotes D diffusion back to the surface enhancing D re-emission.

5. Conclusions

The effect of surface helium on deuterium retention and uptake into the bulk of tungsten was investigated. To quantify the influence of He on D uptake at the surface, we have geometrically separated the three interaction regions, He implantation region, D implantation region and the region beyond both, where D if diffuses further is trapped. This was achieved first by He implantation close to the surface (40 nm) with 3 keV He ions with different fluences and at different temperatures. Samples were exposed to a low flux 300 eV/D ions at 450 K where D implantation range was shallower (15 nm) compared to the He implantation range. Samples were irradiated by 20 MeV W irradiation after He implantation to create defects within the first 2.3 μm. The defects created by W ions were used to trap penetrating D through the He surface layer and make it hence possible to quantify D transport beyond the He layer using ^{3}He nuclear reaction analysis. The same D ion fluence was applied to all samples also to a reference no-He sample, with only W irradiation, so that the D uptake at the He layer and beyond this layer could be quantified. Elastic recoil detection analysis enabled us to measure the D and He concentration depth profiles near the surface. With the same D fluence the W-irradiated layer in only W-irradiated W sample was populated by D down to 3 μm whereas for the samples irradiated by He, the total D retention was four times lower and 15 times less D retention was observed beyond the 40 nm. Microstructure of He-irradiated samples was analysed by TEM showing 1–3 nm big He bubbles. Results show that D gets preferentially retained where He is implanted with D concentrations up to 10 at.%. At the same time implantation beyond the He zone is vastly reduced compared to a He-free W sample. Comparing the present study with our similar methodology applied for bulk transport we can conclude the He microscopy structure promotes D diffusion back to the surface which enhances D re-emission and the observed D retention in He irradiated samples is due to D trapping at He bubbles.

CRediT authorship contribution statement

S. Markelj: Writing – original draft, Resources, Methodology, Investigation, Formal analysis, Data curation, Conceptualization. **T. Schwarz-Selinger:** Writing – review & editing, Investigation, Formal analysis, Conceptualization. **A. Šestan:** Writing – review & editing, Investigation, Formal analysis. **J. Zavašnik:** Writing – review & editing, Investigation, Formal analysis. **M. Kelemen:** Investigation, Formal analysis.

Declaration of competing interest

The authors declare that they have no known competing financial interests or personal relationships that could have appeared to influence the work reported in this paper.

Acknowledgment

We would like to thank to dr. P. Vavpetič at Jožef Stefan Institute and T. Dürbeck, J. Dorner and M. Fußeder at Max-Planck-Institut für Plasmaphysik for their technical support.

This work has been carried out within the framework of the EUROfusion Consortium and has received funding from the Euratom research and training programme 2014-2018 and 2019-2020 under grant agreement No 633053. The views and opinions expressed herein do not necessarily reflect those of the European Commission. The authors acknowledge the support from the Slovenian Research Agency (research core funding No. P2-0405). This work was supported by IAEA Coordinated Research Project F43025, entitled 'Hydrogen Permeation in Fusion-Relevant Materials'.

Data availability

Data will be made available on request.

References

[1] M. Gilbert, S. Dudarev, D. Nguyen-Manh, S. Zheng, L. Packer, J.-C. Sublet, Neutron-induced dpa, transmutations, gas production, and helium embrittlement of fusion materials, J. Nucl. Mater. 442 (2013) S755–S760.
[2] H. Ullmaier, The influence of helium on the bulk properties of fusion reactor structural materials, Nucl. Fusion 24 (1984) 1039.
[3] M. Shimada, B. Merrill, Tritium decay helium-3 effects in tungsten, Nucl. Mater. Energy 12 (2017) 699–702.
[4] M. Gilbert, J.-C. Sublet, Neutron-induced transmutation effects in W and W-alloys in a fusion environment, Nucl. Fusion 51 (2011) 043005.
[5] S. Markelj, et al., Deuterium transport and retention in the bulk of tungsten containing helium: the effect of helium concentration and microstructure, Nucl. Fusion 60 (2020) 106029.
[6] M. Baldwin, R. Doerner, W. Wampler, D. Nishijima, T. Lynch, M. Miyamoto, Effect of He on D retention in W exposed to low-energy, high-fluence (D, He, Ar) mixture plasmas, Nucl. Fusion 51 (2011) 103021.
[7] M. Miyamoto, S. Mikami, H. Nagashima, N. Iijima, D. Nishijima, R. Doerner, N. Yoshida, H. Watanabe, Y. Ueda, A. Sagara, Systematic investigation of the formation behavior of helium bubbles in tungsten, J. Nucl. Mater. 463 (2015) 3.
[8] Y. Ueda, M. Fukumoto, J. Yoshida, Y. Ohtsuka, R. Akiyoshi, H. Iwakiri, N. Yoshida, Simultaneous irradiation effects of hydrogen and helium ions on tungsten, J. Nucl. Mater. 386–388 (2009) 725–728.
[9] V. Alimov, W. Shu, J. Roth, K. Sugiyama, S. Lindig, M. Balden, K. Isobe, T. Yamanishi, Surface morphology and deuterium retention in tungsten exposed to low-energy, high flux pure and helium-seeded deuterium plasmas, Phys. Scr. T138 (2009) 014048.
[10] H. Lee, A. Haasz, J. Davis, R. Macaulay-Newcombe, Hydrogen and helium trapping in tungsten under single and sequential irradiations, J. Nucl. Mater. 360 (2007) 196–207.
[11] M. Baldwin, R. Doerner, Hydrogen isotope transport across tungsten surfaces exposed to a fusion relevant He ion fluence, Nucl. Fusion 57 (2017) 076031.
[12] M. Ialovega, E. Bernard, R. Bisson, C. Martin, R. Sakamoto, A. Kreter, E. Hodille, T. Angot, C. Grisolia, Hydrogen trapping in tungsten: impact of helium irradiation and thermal cycling, Phys. Scr. T171 (2020) 014066.
[13] H. Iwakiri, K. Morishita, N. Yoshida, Effects of helium bombardment on the deuterium behavior in tungsten, J. Nucl. Mater. 307–311 (2002) 135–138.
[14] I. Arkhipov, S. Kanashenko, V. Sharapov, R. Zalavutdinov, A. Gorodetsky, Deuterium trapping in ion-damaged tungsten single crystal, J. Nucl. Mater. 363–365 (2007) 1168–1172.

[15] G. Shaw, W. Garcia, X. Hu, B. Wirth, Investigating helium–deuterium synergies in plasma-exposed tungsten using laser ablation techniques, Phys. Scr. T171 (2020) 014029.
[16] M. Miyamoto, K. Sano, T. Sawae, M. aruta and H. Kurata, Effect of helium irradiation on the hydrogen isotope retention in tungsten by in situ TEM and STEM-EELS analysis, Nucl. Mater. Energy 36 (2023) 101484.
[17] C. Becquart, C. Domain, A density functional theory assessment of the clustering behaviour of He and H in tungsten, J. Nucl. Mater. 386–388 (2009) 109–111.
[18] H.-B. Zhou, Y.-L. Liu, S. Jin, Y. Zhang, G.-N. Luo, G.-H. Lu, Towards suppressing H blistering by investigating the physical origin of the H–He interaction in W, Nucl. Fusion 50 (2010) 115010.
[19] N. Juslin, B. Wirth, Molecular dynamics simulation of the effect of sub-surface helium bubbles on hydrogen retention in tungsten, J. Nucl. Mater. 438 (2013) S1221–S1223.
[20] F. Sefta, K. Hammond, N. Juslin, B. Wirth, Tungsten surface evolution by helium bubble nucleation, growth and rupture, Nucl. Fusion 53 (2013) 073015.
[21] Z. Bergstrom, M. Cusentino, B. Wirth, A Molecular Dynamics Study of Subsurface Hydrogen-Helium Bubbles in Tungsten, Fusion Sci. Technol. 71 (2017) 122–135.
[22] C. Becquart, C. Domain, Migration Energy of He in W Revisited by Ab Initio Calculations, Phys. Rev. Lett. 97 (2006) 196402.
[23] H.-B. Zhou, Y.-H. Li, G.-H. Lu, Modeling and simulation of helium behavior in tungsten: a first-principles investigation, Comput. Mater. Sci 112 (2016) 487–491.
[24] K. Hammond, Helium, hydrogen, and fuzz in plasma-facing materials, Mater. Res. Express 4 (2017) 104002.
[25] A. Manhard, M. Balden, S. Elgeti, Quantitative Microstructure and defect Density Analysis of Polycrystalline Tungsten Reference Samples after Different Heat Treatments, Pract. Metallorg. 52 (2015) 437.
[26] A. Manhard, G. Matern, M. Balden, A Step-By-step Analysis of the Polishing Process for Tungsten Specimens, Pract. Metallorg. 50 (2013) 5–16.
[27] S. Markelj, M. Pečovnik, T. Schwarz-Selinger, M. Kelemen, The synergies between displacement damage creation and hydrogen presence: the effect of D ion energy and flux, Phys. Scr. 97 (2022) 024006.
[28] J. Ziegler, "www.srim.org.," [Online].
[29] T. Schwarz-Selinger, Deuterium Retention in MeV Self-Implanted Tungsten: Influence of Damaging Dose Rate, Nuclear Energy and Materials 12 (2017) 683–688.
[30] ASTM Int'l E521-16, "Standard practice for neutron radiation damage simulation by charge-particle irradiation," in *Annual Book of ASTM Standards vol 12.02*, Philadelphia, PA, American Society for Testing and Materials, 2016, p. p 8.
[31] O.V. Ogorodnikova, V. Gann, Simulation of neutron-induced damage in tungsten by irradiation with energetic self-ions, J. Nucl. Mater. 460 (2015) 60.
[32] V. Alimov, Y. Hatano, B. Tyburska-Püschel, K. Sugiyama, I. Takagi, Y. Furuta, J. Dorner, M. Fußeder, K. Isobe, T. Yamanishi, M. Matsuyama, Deuterium retention in tungsten damaged with W ions to various damage levels, J. Nucl. Mater. 441 (2013) 280–285.
[33] T. Schwarz-Selinger, A critical review of experiments on deuterium retention in displacement-damaged tungsten as function of damaging dose, Mater. Res. Express 10 (2023) 102002.
[34] S. Markelj, et al., Displacement damage stabilization by hydrogen presence under simultaneous W ion damage and D ion exposure, Nucl. Fusion 59 (2019) 086050.
[35] B. Wielunska, M. Mayer, T. Schwarz-Selinger, U. von Toussaint, J. Bauer, Cross Section Data for the D(3He,p)4He Nuclear Reaction from 0.25 to 6MeV, Nucl. Instrum. Methods Phys. Res., Sect. B 371 (2016) 41–45.
[36] M. Mayer, E. Gauthier, S. K, U. v. Toussaint, Nucl. Instr. and Meth. in Phys. Res. B 267 (2009) 506.
[37] M. Meyer, "SIMNRA User's Guide, Report IPP 9/113," Max-Planck-Instutut für Plasmaphysik, Garching, Germany, Available: http://www.rzg.mpg.de/~mam/., 1997.
[38] K. Schmid, U. von Toussaint, Nucl, *Instr. and Meth. in Phys*, Res. B 281 (2012) 64.
[39] A. Kärcher, T. Schwarz-Selinger, V. Burwitz, L. Mathes, C. Hugenschmidt, W. Jacob, The influence of displacement damage on helium uptake and retention in tungsten, Nuclear Materials and Energy 34 (2023) 101370.
[40] C.A. Schneider, W.S. Rasband, NIH image to ImageJ: 25 Years of image Analysis, Nat. Methods 9 (2012) 671.
[41] J. Zavašnik, A. Šestan, V. Shvalya, Chapter Seven - Microscopic techniques for the characterisation of metal-based nanoparticles, Elsevier, Comprehensive Analytical Chemistry, 2021.